

Article

# Advanced Medical Image Segmentation Enhancement: A Particle-Swarm-Optimization-Based Histogram Equalization Approach

Shoffan Saifullah <sup>1,2,\*</sup>  and Rafał Dreżewski <sup>1,3</sup> <sup>1</sup> Faculty of Computer Science, AGH University of Krakow, 30-059 Krakow, Poland; drezew@agh.edu.pl<sup>2</sup> Department of Informatics, Universitas Pembangunan Nasional Veteran Yogyakarta, Yogyakarta 55281, Indonesia<sup>3</sup> Artificial Intelligence Research Group (AIRG), Informatics Department, Faculty of Industrial Technology, Universitas Ahmad Dahlan, Yogyakarta 55166, Indonesia

\* Correspondence: shoffans@upnyk.ac.id

**Abstract:** Accurate medical image segmentation is paramount for precise diagnosis and treatment in modern healthcare. This research presents a comprehensive study of the efficacy of particle swarm optimization (PSO) combined with histogram equalization (HE) preprocessing for medical image segmentation, focusing on lung CT scan and chest X-ray datasets. Best-cost values reveal the PSO algorithm's performance, with HE preprocessing demonstrating significant stabilization and enhanced convergence, particularly for complex lung CT scan images. Evaluation metrics, including accuracy, precision, recall, F1-score/Dice, specificity, and Jaccard, show substantial improvements with HE preprocessing, emphasizing its impact on segmentation accuracy. Comparative analyses against alternative methods, such as Otsu, Watershed, and K-means, confirm the competitiveness of the PSO-HE approach, especially for chest X-ray images. The study also underscores the positive influence of preprocessing on image clarity and precision. These findings highlight the promise of the PSO-HE approach for advancing the accuracy and reliability of medical image segmentation and pave the way for further research and method integration to enhance this critical healthcare application.



**Citation:** Saifullah, S.; Dreżewski, R. Advanced Medical Image Segmentation Enhancement: A Particle-Swarm-Optimization-Based Histogram Equalization Approach. *Appl. Sci.* **2024**, *14*, 923. <https://doi.org/10.3390/app14020923>

Academic Editors: Zongwei Zhou, Hongming Shan and Ruibin Feng

Received: 31 December 2023

Revised: 17 January 2024

Accepted: 19 January 2024

Published: 22 January 2024



**Copyright:** © 2024 by the authors. Licensee MDPI, Basel, Switzerland. This article is an open access article distributed under the terms and conditions of the Creative Commons Attribution (CC BY) license (<https://creativecommons.org/licenses/by/4.0/>).

**Keywords:** medical image enhancement; particle swarm optimization (PSO); histogram equalization; medical imaging

## 1. Introduction

Medical image segmentation is a critical component of modern healthcare [1] that enables clinicians and researchers to extract valuable insights from complex visual data [2,3]. Accurate and reliable segmentation is vital for tasks such as disease diagnosis, treatment planning, and the assessment of treatment outcomes [4–7]. However, the inherent challenges in this process, including noise, non-uniform illumination, and variations in tissue intensity, have spurred ongoing research to find more effective techniques [8–10].

Medical images acquired through techniques like MRI, CT scan, and X-ray [11] often exhibit variations in contrast, brightness, and texture [12]. These variations can obscure critical anatomical structures and pathologies, making accurate segmentation a formidable task [13,14]. Conventional segmentation methods such as thresholding, region growing [15,16], and active contour [17] struggle to produce reliable results in the face of such complexities [18]. Therefore, there is an urgent need for advanced techniques capable of handling these challenges with precision [19,20].

This article presents an innovative approach to address these challenges and offers a sophisticated solution for advancing medical image segmentation [21]. Our method harnesses the power of particle swarm optimization (PSO) [22] in conjunction with histogram equalization (HE) [23] with the aim of significantly enhancing the accuracy and robustness

of image segmentation in the medical domain. PSO emerges as a promising optimization framework for addressing the intricacies of medical image segmentation [24,25]. Inspired by the collective behavior of swarming particles, PSO excels at finding optimal solutions in complex, multidimensional spaces [26]. By adapting PSO to the task of medical image segmentation [27,28], we aim to exploit its ability to converge toward the most suitable image partitioning considering both global and local characteristics. Histogram equalization (HE) is a well-established image enhancement technique that adjusts the pixel intensities to achieve a more uniform distribution, thereby improving contrast and mitigating the effects of non-uniform illumination [29]. Integrating HE into our approach complements the optimization capabilities of PSO by preparing the input images for segmentation by enhancing the visibility of critical details within medical images.

What sets our approach apart is the synergistic fusion of PSO and HE. PSO optimizes the segmentation process by finding an optimal partitioning of the image [30], while HE preprocesses the image to enhance contrast and visibility [31]. This combination addresses the dual challenges of accurately identifying regions of interest and improving image quality, resulting in a more robust and precise segmentation method. In this article, we delve into the theoretical underpinnings of PSO and HE to provide in-depth insights into their integration. Furthermore, we present empirical evidence of the effectiveness of our approach through extensive experiments and comparisons with existing methods. We aim to demonstrate the novelty of our approach and its practical significance, and offer a potential paradigm shift in medical image analysis.

This article is structured in five main sections. Section 1 provides an overview of the significance of medical image segmentation and its challenges. In Section 2, we review previous research, identify gaps in existing methodologies, and establish the context for our study. Section 3 presents the core method, where we combine particle swarm optimization (PSO) with histogram equalization (HE). This section explains the technical aspects of our approach. In Section 4, we analyze empirical findings and their implications. Finally, Section 5 summarizes the key points and discusses their potential impact on healthcare.

## 2. Related Works

The field of medical image segmentation has witnessed significant progress, with numerous approaches having been developed to address the challenges presented by diverse medical imaging scenarios [32,33]. In this section, we provide an overview of the relevant literature that lays the foundation for our novel particle swarm optimization (PSO)-based histogram equalization (HE) approach.

### 2.1. Traditional Segmentation Methods

Traditional segmentation methods have historically served as the building blocks of medical image analysis [32,34]. These methods include thresholding, region growing, and edge detection [35–37]. Researchers conducted a comparative study of thresholding techniques for medical image segmentation [34,38] and highlighted their simplicity and limitations in handling complex intensity variations [39]. One facet of the research community has explored the challenges and prospects of region-growing-based segmentation [40], particularly in complex structures like brain tumor images [41,42]. This exploration has led to a recognized need for more robust techniques to address the subtleties and complexities of such images [43].

Furthermore, foundational knowledge of digital image processing has underpinned many traditional segmentation methods [44]. However, it is crucial to acknowledge that these traditional techniques often face difficulties when handling noisy or non-uniformly illuminated images [45,46]. This recognition has driven the exploration for more advanced and adaptable approaches.

## 2.2. Enhancement Techniques

Enhancement techniques are pivotal for elevating image quality and facilitating subsequent segmentation processes [47]. These techniques aim to enhance contrast and improve overall image visibility in order to contribute to more effective segmentation outcomes [48,49].

One avenue of research explores the enhancement of medical image segmentation through adaptive histogram equalization [50], highlighting its potential for contrast improvement [23,29,51]. Additionally, a comprehensive survey has delved into image enhancement techniques within medical imaging [52]. This survey provides valuable insights into various methods to address challenges such as non-uniform illumination and noise in medical images [53]. This foundational overview of image enhancement techniques is essential for understanding strategies to improve the quality of medical images prior to the segmentation process.

## 2.3. Optimization-Based Approaches

Optimization-based methods have gained significant attention for advanced medical image segmentation enhancement [54,55]. These approaches are designed to fine-tune and optimize segmentation algorithms [22], which aligns with the core objectives of our study. By leveraging optimization strategies, these methods hold the promise of enhancing the accuracy and efficiency of medical image segmentation [56,57], which aligns with the central theme of our research: “Advanced Medical Image Segmentation Enhancement (AMISE): The PSO-Based HE Approach”.

Through a comprehensive exploration of optimization-based approaches conducted by various researchers, their relevance for enhancing the AMISE approach becomes evident. This review encompasses a broad spectrum of optimization strategies, including traditional optimization algorithms, metaheuristic approaches, and machine-learning-based optimization [58–60], all of which resonate with the innovative and advanced nature of our proposed method. These techniques aim to address the intricate challenges of medical image segmentation and to ultimately optimize algorithm parameters to improve the segmentation outcomes, and, by extension [24,33], to advance the core concept of image enhancement that underpins our research.

The significance of optimization-based approaches aligns with the primary objective of our study, which is to refine and advance medical image segmentation through the AMISE approach. By optimizing segmentation algorithms, these techniques contribute to the precise delineation of regions of interest within medical images [61]. Thus, they directly pertain to our research’s fundamental goal of advancing medical image segmentation by integrating particle swarm optimization and histogram equalization and offer a valuable perspective into the strategies used to achieve this enhancement.

## 2.4. Particle Swarm Optimization (PSO) in Image Analysis

Particle swarm optimization (PSO) has emerged as a versatile and innovative optimization technique, with applications spanning various domains, including image analysis [62,63]. Initially conceived as an optimization method inspired by collective swarm behavior, PSO’s adaptability, effectiveness, and problem-solving capabilities make it an increasingly influential tool in image analysis [64,65]. Within the broader context of image analysis, PSO excels at tasks such as feature selection [66], image registration [67], image segmentation [68–70], and object tracking [71]. Its capacity to navigate complex search spaces and avoid local optima positions it as an attractive choice for researchers.

In medical image analysis, our research takes a pioneering step by extending the application of PSO to the specific realm of medical image segmentation [59]. This strategic extension capitalizes on PSO’s inherent strengths in exploring intricate search spaces: aligning seamlessly with the complexities often encountered in medical images, which are marked by noise, non-uniform illumination, and intricate structures [72]. Understanding the pivotal role of PSO in image analysis forms the cornerstone of our research, wherein we

harness its unique optimization capabilities to refine and enhance the accuracy of medical image segmentation as outlined in “AMISE: PSO-Based HE Approach”.

### 2.5. Fusion of Optimization and Image Enhancement

The fusion of optimization techniques with image enhancement methods signifies a rapidly evolving research area with significant implications for medical image analysis [16,73,74]. This emerging field explores the seamless integration of optimization strategies and image enhancement techniques to collectively address the challenges encountered in medical image segmentation [75]. Notably, it highlights the potential of optimization-enhanced approaches to substantially improve segmentation accuracy, particularly for extracting critical structures such as brain tumors from MRI images [76]. This avenue of research has yielded methods that enhance the visibility of structures within medical images while concurrently optimizing the precise delineation of regions of interest [77].

At the same time, the growing interest in machine learning techniques and their application within the medical imaging domain has provided valuable insights into their role in computer-aided diagnosis and deep-learning-based image segmentation [78]. These advances have catalyzed innovation in image analysis techniques and offer valuable perspectives for addressing the complexities presented by intricate medical images [79]. However, deep learning for medical image analysis presents challenges due to computational cost and processing time, along with an increased risk of overfitting due to limited data [80]. Our research builds upon this evolving body of knowledge by introducing a pioneering approach that synergizes PSO and HE to enhance medical image segmentation. In the following sections, we delve into the technical intricacies of our proposed method and present empirical findings: presenting a fresh and innovative perspective to address the challenges associated with noisy and non-uniform medical images.

## 3. Materials and Methods

In this section, we describe the method employed in our novel approach, which combines particle swarm optimization (PSO) with histogram equalization (HE) to enhance medical image segmentation. We outline the critical steps involved in the proposed method, including data preprocessing, PSO-based optimization, and integration with HE. The detailed process can be seen in Figure 1.

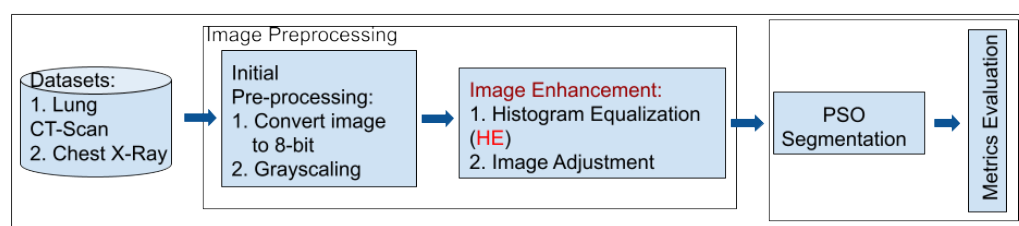


**Figure 1.** Overview of the proposed PSO-HE approach for enhanced medical image segmentation.

### 3.1. Dataset Selection

Our study leverages two distinct datasets (lung CT scan dataset and chest X-ray (COVID-19) dataset), each carefully chosen to represent different aspects of medical imaging challenges and diagnostic scenarios.

#### 3.1.1. Lung CT Scan Dataset [81]

The lung CT scan dataset consists of a total of 267 medical images. These images are representative of lung CT scans—a common modality used in pulmonary imaging. Lung CT scans provide high-resolution cross-sectional views of the chest, making them essential for diagnosing various respiratory conditions and diseases (Figure 2).

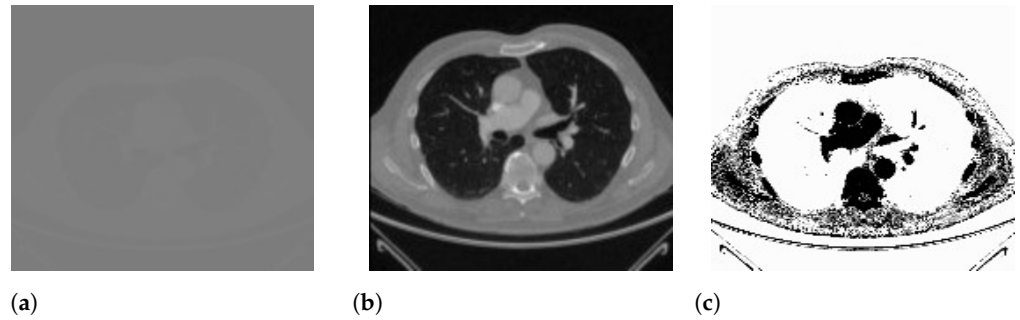


**Figure 2.** Sample of lung CT scan image: (a) original image and (b) the high-resolution image from the dataset with (c) its complement.

To ensure comprehensive evaluation of our method’s performance, we purposefully chose datasets with unique characteristics and challenges, such as the lung CT scan dataset. This dataset primarily comprises high-resolution CT scan images of the lungs, which are known for their intricate anatomical structures, including lung parenchyma, blood vessels, and airways. Challenges encountered within this dataset encompass the identification of subtle abnormalities, the management of variations in lung density, and the requirement for precise segmentation of lung regions.

### 3.1.2. Chest X-ray (COVID-19) Dataset [82]

The chest X-ray dataset encompasses a larger collection of 3616 images. These images are chest X-rays (Figure 3)—a fundamental diagnostic tool widely used in clinical practice. This dataset reflects a diverse range of medical conditions, including those related to COVID-19 [83], and includes a variety of anatomical regions within the chest.



**Figure 3.** Sample chest X-ray images with different classes: (a) normal, (b) COVID-19, (c) lung opacity, and (d) pneumonia.

As mentioned above, we chose datasets with different characteristics and challenges to evaluate our method’s performance. The chest X-ray dataset, for instance, consists of 2D X-ray images of the chest. These images introduce a unique set of challenges, characterized by lower spatial resolution and the presence of overlapping structures such as ribs and organs. Moreover, these images, relevant to COVID-19 diagnosis, might exhibit specific patterns associated with viral pneumonia, adding another layer of complexity to the segmentation process.

### 3.1.3. Ground-Truth Annotations

In order to rigorously assess the performance of our segmentation method, we relied on meticulously generated ground-truth annotations. These annotations provide a critical reference point for evaluating the accuracy and effectiveness of our approach at delineating regions of interest within the medical images.

Our ground-truth data was collected from Kaggle [81,82], which is a reputable platform for data sharing and collaboration. The annotations were crafted and meticulously reviewed by medical experts who possess specialized knowledge in the relevant domains. These experts conducted the labor-intensive task of manually outlining regions of clinical significance in the medical images, ensuring that structures and areas crucial for clinical

diagnoses were precisely identified. The GT images in Figure 4 exemplify samples of these annotations and showcase the quality of the reference data from both the lung CT scan and chest X-ray datasets. These ground-truth figures serve as invaluable benchmarks that enable us to quantitatively measure the method's accuracy at segmenting regions of interest within the medical images.

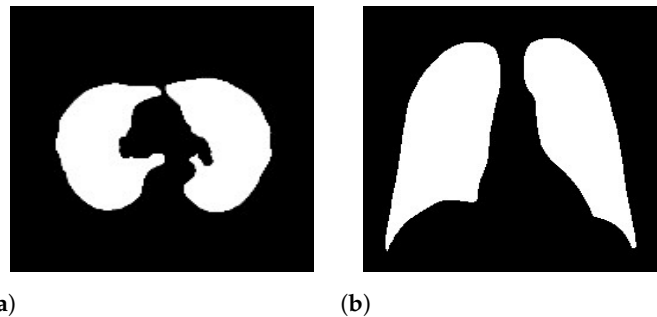


**Figure 4.** Sample ground-truth (GT) annotations from the (a) lung CT scan and (b) chest X-ray COVID-19 datasets.

The utilization of these rigorously sourced and expert-validated ground-truth data is of paramount importance. They offer a trustworthy foundation for evaluating the quality of our segmentation results, ensuring that our approach aligns with clinical standards and expert assessments. This alignment is essential for determining the effectiveness of our proposed PSO-based method for real-world medical image analysis.

### 3.2. Dataset Preprocessing

Data preprocessing is crucial for ensuring that the input medical images are optimal for subsequent segmentation and enhancement processes [84]. The preprocessing steps address image artifacts, enhance image quality, and simplify image representation [85]. In this section, we provide a comprehensive description of the data preprocessing pipeline, which includes the following key steps: image conversion to 8-bit, grayscaling, image enhancement with histogram equalization (HE), and image adjustment. These methods can improve the quality of images without any information being deformed or lost [86].

#### 3.2.1. Image Conversion to 8-bit

The initial step in data preprocessing involves converting the raw medical images into an 8-bit format [87]. This conversion simplifies the pixel intensity values to a range between 0 and 255, which is more manageable for subsequent processing. The 8-bit representation ensures uniformity across all images, regardless of their original bit depths [88]. This simplification is particularly important for consistency in the analysis and facilitates efficient memory usage.

#### 3.2.2. Grayscaling

Following 8-bit conversion, the images are grayscaled, ensuring that they are represented in grayscale intensity levels [89]. Grayscaling simplifies the images by reducing them to a single channel, which eliminates color information. This simplification reduces computational complexity and memory requirements while preserving essential intensity information [90]. Grayscaling is a fundamental preprocessing step that ensures uniformity in the image data and simplifies subsequent processing [91].

#### 3.2.3. Image Enhancement with Histogram Equalization (HE)

One of the central aspects of data preprocessing is the application of histogram equalization (HE). This enhancement technique redistributes pixel intensities to achieve a more uniform histogram [92]. Histogram equalization (HE) is employed to improve the contrast and visibility of structures within the images [93]. By enhancing fine details and mitigating

non-uniform illumination, HE prepares the images for more accurate segmentation. This step is crucial for ensuring that subtle features and structures are well-visualized and can be accurately delineated during subsequent processing.

### 3.2.4. Image Adjustment

In addition to the above steps, image adjustment techniques are applied to fine-tune specific image properties. These adjustments may include brightness and contrast adjustments to optimize the visual representation of the images. Image adjustment ensures that the preprocessed images are well-suited for subsequent segmentation and optimization processes by fine-tuning the image properties to achieve optimal visualization.

### 3.3. Particle Swarm Optimization (PSO)

Particle swarm optimization (PSO) is a powerful optimization technique inspired by the collective behavior of swarming particles [94]. It has gained prominence in various fields, including image analysis and medical image segmentation, due to its ability to efficiently explore complex search spaces and find optimal solutions. In this section, we provide an in-depth description of the application of PSO in our method for medical image segmentation.

At the core of PSO lies the concept of simulating the social behavior of particles within a swarm. Each particle in the swarm represents a potential solution to an optimization problem [95]. The behavior of particles is guided by their positions and velocities in a multidimensional search space. PSO has been widely applied in image analysis tasks, including image registration, feature selection, and image segmentation [96]. In the context of medical imaging, PSO is particularly valuable due to its ability to address the challenges posed by noisy and complex images [97]. Its capacity to explore complex, multidimensional spaces efficiently makes it a valuable tool for optimizing image processing and segmentation algorithms.

The core of our method lies in the utilization of particle swarm optimization (PSO) to optimize the image segmentation process. The PSO algorithm is applied to partition the preprocessed image into distinct regions. The steps involved in PSO-based segmentation (Figure 5) are as follows:

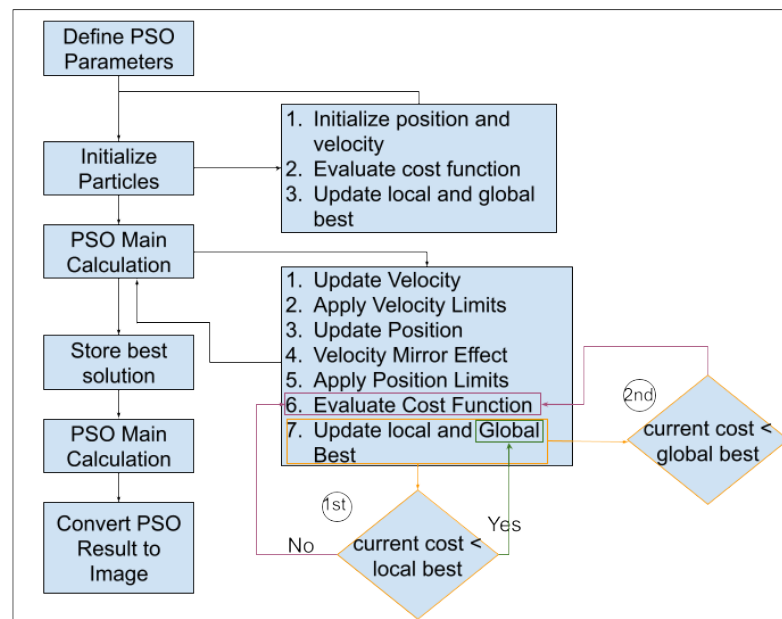


**Figure 5.** Flowchart of the proposed particle swarm optimization (PSO) algorithm for medical image segmentation based on updated parameters.

- (a) **Particle Initialization:** We initialize a swarm of particles, wherein each particle represents a potential segmentation solution. The particles are assigned positions in the search space corresponding to potential image partitions. In the context of medical image segmentation, each partition represents a potential delineation between regions of interest within the image.
- (b) **Objective Function:** We define an objective function (Equation (1)) that quantifies the quality of a given image partition. The objective function considers factors such as intensity, gradient information, and region connectivity. The goal is to find the partition that minimizes this function—effectively identifying the optimal image segmentation.

$$f(X) = w_1 \times \text{Intensity}(X) + w_2 \times \text{Gradient}(X) + w_3 \times \text{Connectivity}(X) \quad (1)$$

- **Intensity Component:** The intensity term ( $w_1 \times \text{Intensity}(X)$ ) gauges the distribution and variation of pixel intensities within the image partition. Higher  $w_1$  values amplify the emphasis on the intensity, making it a pivotal factor for distinguishing regions based on pixel brightness. This ensures that the segmentation process prioritizes areas with distinct intensity characteristics.
- **Gradient Information Component:** The gradient information term ( $w_2 \times \text{Gradient}(X)$ ) delves into the spatial variations in pixel intensities, emphasizing edges and boundaries. A higher  $w_2$  amplifies the influence of gradient information in the objective function, steering the segmentation towards regions with pronounced transitions in pixel values. This is crucial for preserving fine details and outlining distinct structures within the image.
- **Region Connectivity Component:** The region connectivity term ( $w_3 \times \text{Connectivity}(X)$ ) assesses the coherence and connectivity between adjacent pixels within the partition. Increasing  $w_3$  intensifies the significance of region connectivity in the overall objective function, guiding the segmentation process towards creating contiguous and meaningful partitions. This ensures that segmented regions exhibit a natural flow and connectivity, enhancing the overall structural integrity of the partition.

The terms  $w_1$ ,  $w_2$ , and  $w_3$  are weights assigned to each measure to adjust their influence on the overall objective function. The optimization goal is to find the optimal partition by minimizing  $f(X)$ .

- (c) **Optimization Iterations:** The PSO algorithm iteratively updates the positions of particles based on their previous best positions and the best positions found by neighboring particles. Particles adjust their positions in search of the optimal image partition. The optimization continues until convergence criteria are met or a specified number of iterations is reached. Each particle keeps track of two pivotal fitness values: “local best (pbest)” (Equation (2)) and “global best (gbest)” (Equation (3)) [95]. The term “pbest” signifies the best value achieved by an individual particle throughout the optimization process and is recalculated iteratively at each time step. In contrast, “global best” represents the overarching best value attained among all particles’ “pbest” values up to that specific time step.

$$\mathbf{p}_{best_i}^t = \mathbf{x}_i^* \mid f(\mathbf{x}_i^*) = \min_{k=1,2,\dots,t} \left( \left\{ f(\mathbf{x}_i^k) \right\} \right), \text{ where } (i \in \{1, 2, \dots, N\}) \quad (2)$$

$$\mathbf{g}_{best}^t = \mathbf{x}_*^t \mid f(\mathbf{x}_*^t) = \min_{\substack{i=1,2,\dots,N \\ k=1,2,\dots,t}} \left( \left\{ f(\mathbf{x}_i^k) \right\} \right) \quad (3)$$

In optimization [98],  $i$  represents the particle’s index (1 to  $N$ ),  $t$  is the current iteration,  $f$  is the objective function to be minimized,  $x$  is the position vector, and  $N$  is the total number of particles in the swarm.

- (d) **Optimal Partition Extraction:** The final result of PSO is the image partition that minimizes the objective function. This partition represents segmentation of the input

medical image into distinct regions of interest. The partition is chosen based on the collective behavior of particles, which adapt and explore the search space to find the best segmentation. Particle positions and velocities evolve dynamically based on Equations (4) and (5).

$$X_{(n+1)}^i = X_n^i + V_{(n+1)}^i \quad (4)$$

$$V_{(n+1)}^i = V_n^i + c_1 r_1 (pbest_n^i - X_n^i) + c_2 r_2 (gbest_n^i - X_n^i) \quad (5)$$

In particle swarm optimization (PSO), key variables and parameters shape the optimization process [28]. These include the positions ( $X_n^i$  and  $X_{(n+1)}^i$ ) and velocities ( $V_{(n+1)}^i$ ) of particles as well as essential factors like the inertia weight ( $w$ ), cognitive component ( $c_1$ ), social component ( $c_2$ ), and random values ( $r_1$  and  $r_2$ ) within the range  $[0, 1]$ . Additionally, PSO tracks two significant values:  $pbest_n^i$ , the best position found by a particle at time step  $t$ ; and  $gbest_n^i$ , the best position found across the entire swarm at time step  $t$ . These elements collectively steer particle dynamics and the quest for optimal solutions.

The application of PSO in medical image segmentation offers several advantages, including its ability to handle non-convex and non-linear objective functions [99], its simplicity of implementation, and its capacity to explore a diverse range of solutions. However, like other optimization techniques, PSO is sensitive to its parameter settings and may converge to local optima if not carefully tuned [22,57].

In our method, PSO plays a central role in optimizing the image segmentation process. It is seamlessly integrated with histogram equalization (HE), which enhances the quality of the segmented regions. This integration addresses the limitations associated with traditional segmentation methods and offers a novel and effective solution to the challenges associated with medical image segmentation. By incorporating PSO as a core component, our methods optimize the segmentation process and seek the best partitioning of the input medical image. The synergy between PSO and HE enhances the accuracy and robustness of the segmentation results: ultimately improving the quality of the segmented regions and making them more suitable for subsequent analysis and clinical applications.

### 3.4. Integrating PSO and HE for Image Segmentation

This detailed exploration unravels the intricacies of seamlessly integrating particle swarm optimization (PSO) with histogram equalization (HE) to elevate image segmentation performance. This integration's primary aim is to optimize HE parameters dynamically through the adaptive capabilities of PSO and to foster an intricate interplay between algorithmic components.

#### 3.4.1. Algorithmic Integration and Parameter Dynamics

The main goal of the integration is to ensure algorithmic harmony between PSO and HE. PSO, a robust optimization technique, is harnessed to adjust finely crucial HE parameters such as bin width and intensity distribution. The defining feature is the formulation of the objective function within PSO, which is meticulously designed to encapsulate a quantitative measure of image quality or segmentation performance. This strategic design guides the optimization process toward discovering HE parameter settings that maximize the effectiveness of subsequent segmentation steps. The dynamics of PSO parameters, including the inertia weight ( $w$ ), cognitive component ( $c_1$ ), social component ( $c_2$ ), and maximum iterations, are delicately balanced to orchestrate a seamless dance between exploration and exploitation.

#### 3.4.2. Rationale, Benefits, and Experimental Rigor

The rationale behind this integration is grounded in its capacity to enhance adaptive contrast, which is particularly beneficial for the diverse intensity landscapes found in medical images. This adaptive approach enhances feature discrimination, is vital for accurate segmentation, and addresses the challenge of overfitting commonly associated with

generic enhancement techniques. Rigorous experimental validation becomes paramount, with quantitative metrics scrutinizing segmentation accuracy, precision, recall, and F1-score/Dice. Comparative analyses against traditional methods and alternative enhancement techniques provide nuanced insights into the advantages of PSO-HE integration and substantiate its efficacy across varied contexts.

### 3.4.3. Applications and Considerations

The integrated PSO-HE approach is strategically positioned for applications in medical image segmentation. Its adaptability to intricate details and nuanced intensity variations positions it as a formidable tool for achieving precise segmentation outcomes. As we traverse through the intricacies of the integration, considerations extend beyond algorithmic nuances to encompass the pragmatic realm of computational costs. The optimization of parameter settings not only caters to segmentation quality but also ensures computational efficiency: making the approach practically applicable in real-world scenarios.

## 4. Results and Discussion

In this section, we present the results of our proposed method, which combines particle swarm optimization (PSO) with histogram equalization (HE) to enhance medical image segmentation. We discuss the empirical findings, compare our approach with existing methods, and provide a comprehensive analysis of the outcomes.

### 4.1. Experimental Setup

In this section, we provide a comprehensive overview of the experimental setup used to evaluate the performance of the proposed method. A well-designed experimental setup is crucial for assessing the effectiveness and robustness of our approach.

#### 4.1.1. Preprocessing Parameters

In the preparation of the datasets, a standardized set of preprocessing parameters was meticulously and consistently applied to all images. These preprocessing procedures encompassed the conversion of images into 8-bit format and grayscaling to ensure uniformity in the dataset. Additionally, histogram equalization (HE) and image adjustment parameters were meticulously calibrated to enhance the quality and suitability of images for subsequent segmentation and optimization processes.

The initial step of image conversion into 8-bit format was imperative due to the inherent variability within the dataset. This dataset consisted of images with both 8-bit and 16-bit depths. To maintain uniformity in image representation and facilitate consistent processing, all images were converted into 8-bit format. In the 8-bit representation, each pixel is defined within the range of 0–255, spanning 256 levels, ensuring consistent data quality for subsequent processing.

Moreover, as some datasets featured images with three color channels (despite their appearance being similar to that of grayscale), they were transformed into grayscale representations with a single color channel. This harmonization of image attributes across the dataset facilitated standardized preprocessing procedures, ensuring that all subsequent segmentation and optimization tasks were conducted on images optimized for analysis.

The effectiveness of these preprocessing measures can be visually appreciated in Figure 6, which demonstrates the results of histogram equalization (HE) applied to lung CT scan and chest X-ray images, along with their corresponding histogram distributions. This rigorous preprocessing lays the foundation for achieving consistent and high-quality results in the subsequent medical image segmentation processes, ultimately enhancing the accuracy and reliability of healthcare applications.

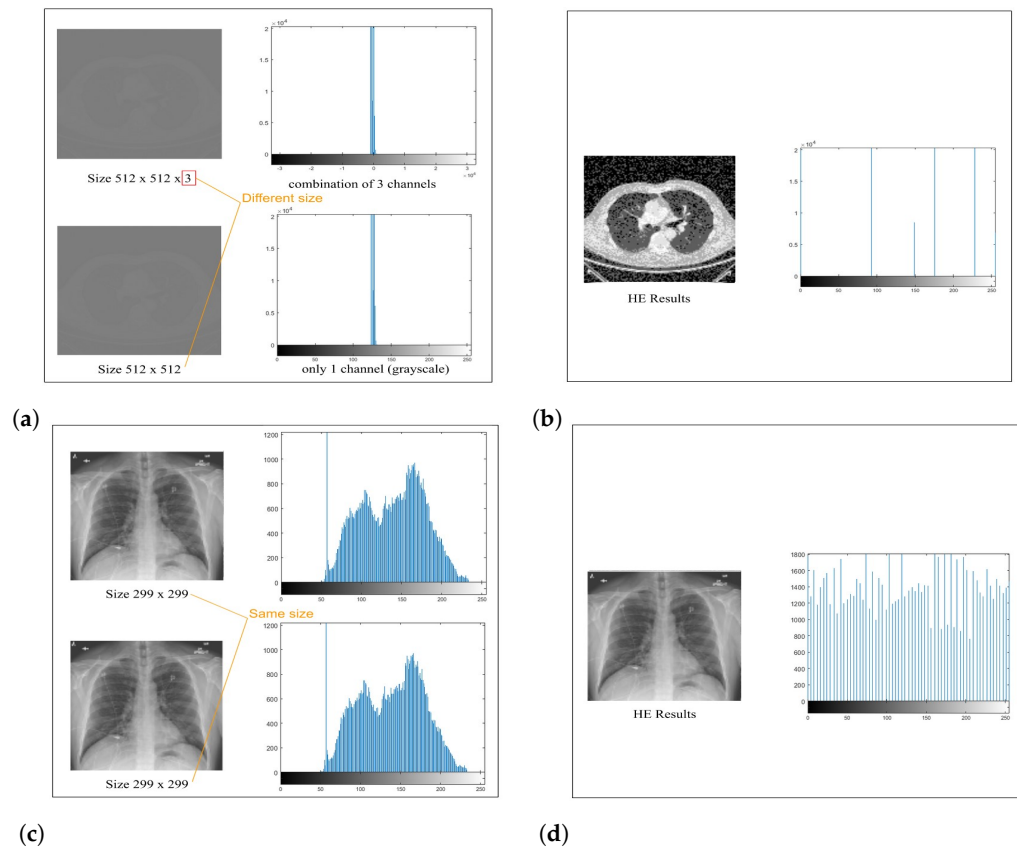


**Figure 6.** Histogram equalization (HE) preprocessing for lung CT scan and chest X-ray images demonstrating the resulting histogram distributions. Grayscaleing 8-bit images of (a) lung CT scan and (c) chest X-ray images followed by HE preprocessing in (b) and (d), respectively, with histograms illustrating the outcome in each case.

Figure 6 highlights significant improvements in image clarity after preprocessing, which are particularly evident in the comparison between Figure 6a,c. Histogram analysis reveals varying distributions in Figure 6a,b, but preprocessing (Figure 6c,d) achieves a uniform distribution through histogram equalization, which enhances overall visual quality and preserves critical details. Our model processing, employing histogram equalization, effectively enhances image clarity and visual quality, which contributes to a more precise depiction of features.

#### 4.1.2. PSO Segmentation Parameters

In our method, we tailor particle swarm optimization (PSO) parameters (Table 1) to the specific characteristics of the datasets and the challenges associated with lung CT scans and chest X-rays. In our experiments, the number of segments ( $k$ ) is a pivotal parameter that determines how the images are partitioned, with  $k$  set to two segments in our experiments. The cost function (*CostFunction*) is the guiding force in the PSO process and directs the partitioning of medical images based on the optimization objective.

The decision variable matrix size (*VarSize*) is specified as  $[k, \text{size}(X, 2)]$  and provides insight into the size of the matrix involved with decision variables. Furthermore, the number of decision variables ( $nVar$ ) is calculated by the product of the dimensions of *VarSize*, which signifies the total number of decision variables considered in the optimization. To ensure that particles adhere to suitable ranges during optimization, we establish lower and upper bounds of variables (*VarMin* and *VarMax*) by considering the minimum and maximum values in the image data.

**Table 1.** PSO segmentation parameters.

Parameter	Description
$k$	Number of segments (set to 2 in experiments): determines image partitioning.
<i>CostFunction</i>	Objective function guiding PSO: minimizes image partitioning quality.
<i>VarSize</i>	Decision variable matrix size, $[k, size(X, 2)]$ : indicates the matrix for decision variables.
$nVar$	Number of decision variables: calculated from <i>VarSize</i> and represents total variables.
<i>VarMin, VarMax</i>	Lower and upper bounds of decision variables based on image data.
<i>MaxIt</i>	Maximum iterations (50): controls optimization duration.
$nPop$	Population size (5): aligned with PSO swarm size.
$w$	Inertia weight (initially 1): balances particle velocity and best-known position.
<i>wdamp</i>	Inertia weight damping (0.99): regulates inertia weight decrease.
$c_1, c_2$	Personal and global learning coefficients (1.5 and 2.5): influence particle movement.
<i>VelMax, VelMin</i>	Velocity limits: preserve particle velocities within bounds.

A series of critical PSO parameters influence the optimization process. Initially, the maximum number of iterations (*MaxIt*) was assessed (with the initial value set to 100) and the population size (*nPop*) varied within the range of 2 to 20 [100] and thereby controlled the duration of the optimization procedure. The optimal iteration was determined by the last iteration in which the minimum best cost function value was achieved and remained unchanged. This criterion is established by the information presented in Figure 5 under the second condition of cost evaluation.

Analysis of the results indicated that setting *MaxIt* to 50 and *nPop* to 5 yielded the optimal outcome, with the best cost of 93.3202. Upon further evaluation, based on the results presented in Figure 7, it was determined that the optimal value for *MaxIt* was 50. Consequently, for subsequent iterations of this experiment, the *MaxIt* parameter was adjusted to 50 to enhance the optimization process. This evaluation also assessed the computation time for each parameter setting, with the aim of minimizing it while achieving the best results. The minimum time recorded was 0.25716 s. These results, including optimal iterations vs. population size and computation time, are presented in Figure 7.

Additionally, we explored scenarios involving the inertia weight ( $w$ ) by varying (decreasing) its value from 1 to 0.4 [101], as shown in Table 2. The results underscore that the optimal weight is 1, as this value demonstrated its effectiveness at achieving optimal outcomes. Optimal results can be obtained with an inertia weight damping ratio (*wdamp*) of 0.99, which dictates how the inertia weight diminishes over each iteration. The personal learning coefficient ( $c_1$ ) and global learning coefficient ( $c_2$ ) are assigned values of 1.5 and 2.5, respectively [102]. These parameters govern the impact of a particle's best-known position and the global best-known position on its movement within the optimization process.

**Table 2.** Experiments for finding parameters of weight ( $w$ ) based on the best-cost values.

Parameters	Experiments						
	1	2	3	4	5	6	7
Weight ( $w$ )	1	0.9	0.8	0.7	0.6	0.5	0.4
Best Cost	93.3202	93.3203	93.3203	93.3204	93.3205	93.3984	93.3725

Velocity limits (*VelMax* and *VelMin*) are instrumental for preserving the velocity of particles within acceptable boundaries. These limits are pivotal for ensuring that particle velocities do not exceed reasonable levels during optimization. By harmonizing these parameters, our method balances exploration and exploitation in order to seek reliable solutions while avoiding overfitting the training data.

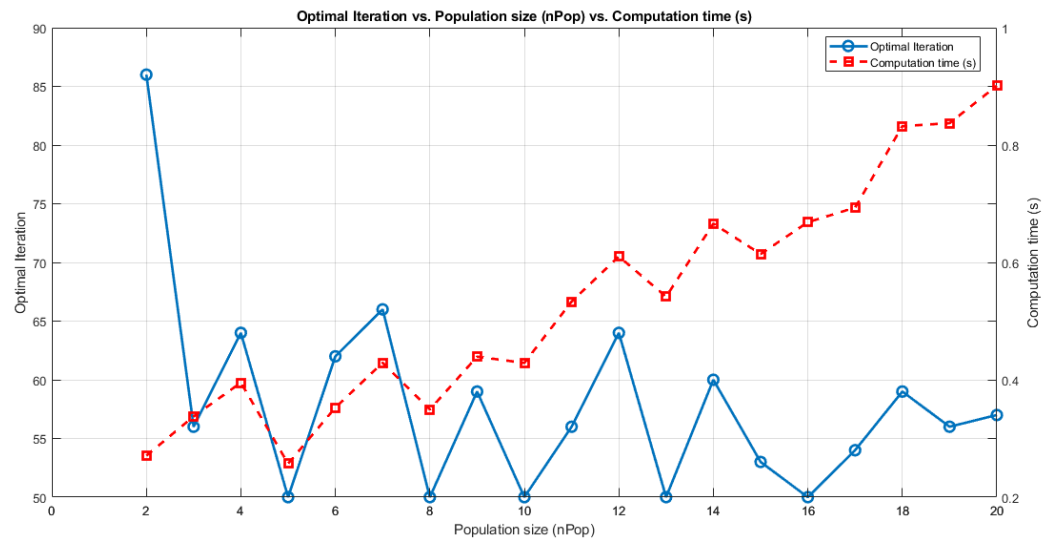


**Figure 7.** Initial process of parameter setting for PSO based on optimal iterations vs. population size (*nPop*) vs. computation time (s). The evaluation was conducted using MATLAB R2023 via Windows 10 Pro 64-bit powered by an Intel Core i7 processor running at 2.9 GHz with eight CPU cores.

#### 4.1.3. Evaluation Metrics

This section assesses the segmentation performance of our particle swarm optimization (PSO) method. We utilize fundamental evaluation metrics to gauge the effectiveness of the PSO-based approach. These metrics provide a detailed perspective on the method’s segmentation precision, recall, and overall accuracy [103]. Accuracy measures the overall precision in classifying regions of interest, while precision evaluates the method’s ability to pinpoint relevant areas with minimal false positives. Recall, also known as sensitivity, examines the effectiveness at capturing all relevant regions. The F1-score, defined as the Dice similarity coefficient (DSC), is a balanced metric that considers both precision and recall to provide an overall performance measure.

Specificity evaluates the method’s capability to exclude non-relevant regions. Overlap-based metrics—the DSC and the Jaccard index (JI)—assess the degree of overlap between the segmented regions and the ground-truth data. These evaluation metrics can be expressed mathematically as follows:

$$Accuracy = \frac{(TP + TN)}{(TP + FP + TN + FN)} \tag{6}$$

$$Precision = \frac{(TP)}{(TP + FP)} \tag{7}$$

$$Recall = \frac{(TP)}{(TP + FN)} \tag{8}$$

$$F1 - Score \text{ or } Dice = \frac{2(Precision \times Recall)}{(Precision + Recall)} = \frac{(2 \times TP)}{2 \times (TP + FP + FN)} \tag{9}$$

$$Specificity = \frac{(TN)}{(TN + FP)} \tag{10}$$

$$JI = \frac{(TP)}{(TP + FP + FN)} \tag{11}$$

This comprehensive array of evaluation metrics offers a holistic perspective of the PSO method’s segmentation quality and alignment with ground-truth data. It allows us to scrutinize its precision, recall, and overall accuracy: thus facilitating a robust evaluation of performance.

## 4.2. Segmentation Performance

Segmentation performance evaluation is a critical aspect of any medical image processing methodology. In this section, we delve into a comprehensive analysis of the particle swarm optimization (PSO) approach's performance when applied to the segmentation of two distinct medical imaging datasets: lung CT scan and chest X-ray. We examine the impact of preprocessing—specifically, histogram equalization (HE)—on the PSO algorithm's performance to investigate its ability to enhance image quality and segmentation accuracy. Furthermore, we compare the outcomes of the PSO segmentation approach with alternative methods such as Otsu, Watershed, and K-means. To achieve a comprehensive evaluation, we consider both quantitative measures and graphical representations, enabling us to gain insights into the method's strengths and limitations when applied to different medical imaging modalities.

The best-cost values and evaluation metrics such as accuracy, precision, recall, F1-score/Dice, specificity, and Jaccard provide a multifaceted assessment of the segmentation quality. This analysis aims to shed light on the effectiveness of the PSO segmentation approach and the significance of selecting appropriate preprocessing techniques tailored to the specific characteristics of each imaging dataset.

### 4.2.1. Analysis of Best-Cost Values

The best-cost values, as depicted in Figure 8, offer valuable insights into the optimization process of the particle swarm optimization (PSO) algorithm applied to medical image segmentation. We consider two distinct datasets, lung CT scan and chest X-ray, each with and without preprocessing using histogram equalization (HE). This analysis aims to understand how different combinations of the PSO algorithm and preprocessing methods influence segmentation convergence behavior and efficiency.

The process initializes a population of particles with random positions and velocities and evaluates their objective function. It updates personal and global best positions based on the cost (Equations (2) and (3)). In the main PSO loop, particle velocities and positions are iteratively updated within imposed limits. The algorithm tracks the best solution and associated information, and incorporates a damping factor for the inertia weight. The process continues for several iterations and stores the final solution and relevant details. The result indicates the indices corresponding to the best solution.

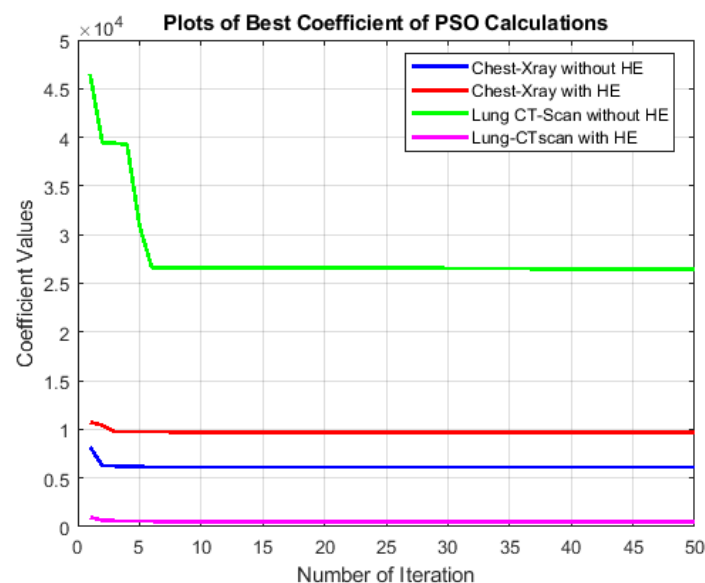


**Figure 8.** Comparison of best-cost values of the PSO segmentation approach for lung CT scan and chest X-ray images with and without histogram equalization (HE) preprocessing.

#### 1. Chest X-ray Segmentation

Without HE, the best-cost values exhibit fluctuations within a relatively narrow range. This indicates that the PSO algorithm converges effectively to a stable solution. The consistency of best-cost values can be attributed to the nature of chest X-ray images, which already possess a certain level of contrast and a grayscale distribution suitable for segmentation. When HE is applied, the best-cost values slightly increase. This is likely due to HE redistribution of pixel intensities and emphasizing the overall contrast, which can create additional complexity in the segmentation process. However, despite the slight increase, the best-cost values remain relatively stable.

#### 2. Lung CT Scan Segmentation

In the case of lung CT scan images, the best-cost values demonstrate more significant variations. Without HE, the algorithm exhibits periodic dips and peaks. The complexity in these images, characterized by intricate anatomical structures like lung parenchyma, blood vessels, and airways, contributes to the periodic fluctuations. These variations might indicate the algorithm's challenges in settling on a precise segmentation solution. With HE preprocessing, the best-cost values exhibit a notable reduction in fluctuations. The redistribution of pixel intensities through HE improves the overall contrast, resulting in a smoother convergence pattern. It is important to note that in this context, a lower best-cost value reflects a more accurate segmentation. The comparison between chest X-ray and lung CT scan datasets highlights the significance of dataset characteristics in influencing the convergence behavior of the PSO algorithm. Moreover, the impact of HE on the optimization process is more pronounced in lung CT scan images, which emphasizes the need for preprocessing methods tailored to the dataset's characteristics.

#### 4.2.2. Analysis of Evaluation Metrics

The detailed examination of the evaluation metrics in Table 3 provides valuable insights into the performance of the PSO segmentation approach in comparison to alternative methods such as Otsu, Watershed, and K-means. These metrics offer a comprehensive understanding of the effectiveness and limitations of each approach in different scenarios, particularly when the histogram equalization (HE) technique is applied.

In Lung CT images without HE, the PSO segmentation approach demonstrates notable performance: achieving an accuracy of 0.91893. This score suggests that it correctly identifies lung structures in these images, as supported by a precision score of 0.90036, which indicates a low rate of false positives. The recall score of 0.97545 emphasizes the ability to capture most relevant structures effectively. The Dice, at 0.9364, strikes a balance between precision and recall. Furthermore, high Dice and Jaccard indices (0.9364 and 0.82984, respectively) reinforce the quality of segmentation.

The sensitivity score of 0.88041 highlights its capacity to identify true positives while maintaining a favorable balance with false positives. These results indicate the strength of the PSO segmentation approach for accurately segmenting lung CT images.

The integration of HE in lung CT images leads to even higher performance, with accuracy of 0.9563 and a Dice value of 0.967. This significant improvement can be attributed to the enhanced contrast and visibility in the images. The Dice and Jaccard indices also witness substantial gains, further underlining the effectiveness of HE. These results underscore the importance of employing HE as a preprocessing step to enhance segmentation accuracy, especially for lung CT images.

In chest X-ray images without HE, the segmentation performance remains commendable, with an accuracy of 0.90335 and a Dice of 0.90202. The precision score of 0.87424 suggests relatively few false positives. The recall score of 0.93162 indicates effective identification of relevant structures. However, the Dice and Jaccard indices slightly drop, reflecting some difficulty in delineating fine details. This can be attributed to the complex nature of chest X-ray images.

**Table 3.** Performance evaluation metrics for the PSO segmentation approach compared to other methods (Otsu, Watershed, and K-means) on medical images, both with and without histogram equalization (HE) preprocessing.

Medical Images	HE	Evaluation Metrics					
		Accuracy	Precision	Recall	Specificity	Dice	Jaccard
<b>PSO Segmentation Approach</b>							
Lung CT	No	0.91893	0.90036	0.97545	0.88041	0.9364	0.82984
Lung CT	Yes	0.9563	0.97529	0.96811	0.93322	0.967	0.9361
Chest X-ray	No	0.9065	0.9350	0.93162	0.87751	0.90202	0.82153
Chest X-ray	Yes	0.90363	0.86891	0.93714	0.87369	0.90173	0.82105
<b>Otsu's Approach</b>							
Lung CT	No	0.91323	0.9422	0.928	0.88283	0.93504	0.87801
Lung CT	Yes	0.91893	0.90036	0.97545	0.88041	0.9364	0.82984
Chest X-ray	No	0.91796	0.88379	0.95155	0.88786	0.91642	0.84573
Chest X-ray	Yes	0.90796	0.92473	0.89751	0.91947	0.91091	0.8364
<b>Watershed Approach</b>							
Lung CT	No	0.87057	0.88893	0.91348	0.79259	0.90104	0.8199
Lung CT	Yes	0.9035	0.94483	0.91266	0.88346	0.92847	0.86649
Chest X-ray	No	0.89371	0.89279	0.89778	0.88954	0.89528	0.81041
Chest X-ray	Yes	0.88755	0.92746	0.86203	0.91842	0.89355	0.80758
<b>K-means Approach</b>							
Lung CT	No	0.82512	0.8654	0.87008	0.73812	0.86773	0.76636
Lung CT	Yes	0.9132	0.94216	0.92799	0.88276	0.93502	0.87798
Chest X-ray	No	0.91754	0.88928	0.94544	0.84587	0.9165	0.89192
Chest X-ray	Yes	0.90794	0.92473	0.89749	0.83638	0.9109	0.91947

The addition of HE to chest X-ray images marginally improves segmentation performance, resulting in an accuracy of 0.90363 and a Dice value of 0.90173. The precision score of 0.86891 implies that it maintains a low false positive rate, and the recall score of 0.93714 indicates effective identification of relevant structures. The Dice and Jaccard indices remain stable, with only slight improvements. It is worth noting that the complexity of chest X-ray images presents inherent challenges for segmentation that even HE cannot entirely mitigate.

When compared to Otsu's segmentation approach, the PSO segmentation approach exhibits competitive performance. This highlights the strength of PSO in medical image segmentation. When compared to the Watershed approach, the PSO segmentation approach consistently outperforms. Watershed, known for over-segmentation issues, lags behind in terms of accuracy and Dice. K-means, an alternative approach, shows comparable performance with the PSO segmentation approach in lung CT images without HE. However, HE significantly enhances K-means' performance, making it a viable alternative. In chest X-ray images, the PSO segmentation approach continues to perform more consistently.

Detailed analysis of the evaluation metrics reveals the PSO segmentation approach's proficiency, especially when HE is applied. The choice of using or not using HE should be tailored to the specific characteristics of the medical images. These insights offer guidance to practitioners for selecting suitable segmentation methods for various medical imaging scenarios. While these results are promising, further research may explore hybrid approaches that combine segmentation algorithms, preprocessing techniques, and machine learning for even more robust and accurate medical image segmentation.

#### 4.3. Segmentation Results Based on Object Cropping

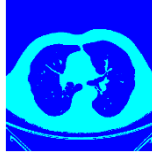
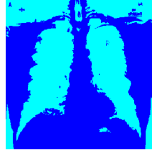
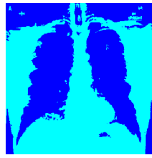
In this section, we focus on segmentation results by specifically examining the cropping of detected objects and comparing them with their corresponding ground-truth images

(GT). We recognize the pivotal role played by preprocessing techniques to enhance the visual quality of segmented images, and we aim to elucidate the profound influence of preprocessing on image clarity and precision. Furthermore, we conducted a comprehensive comparative assessment: evaluating our particle swarm optimization (PSO) approach against alternative segmentation methods, including Otsu, Watershed, and K-means. This multifaceted analysis offers valuable insights into the quality of medical image segmentation achieved by our proposed approach.

#### 4.3.1. Quality Enhancement with Preprocessing

Our exploration begins by emphasizing the critical role of preprocessing for shaping the quality of segmented images. As can be seen from Table 4, images subjected to segmentation without any preprocessing closely resemble their original counterparts. However, the PSO segmentation process introduces scattered noise into the images, potentially obscuring vital image details and diminishing diagnostic accuracy. By contrast, images subjected to preprocessing—notably, employing histogram equalization (HE) and our proposed adjustments—yield substantially improved segmentation outcomes. These preprocessed images exhibit greater clarity and more precise object boundaries.

**Table 4.** Comparative analysis of medical image segmentation results using PSO segmentation with and without histogram equalization (HE) preprocessing.

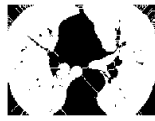
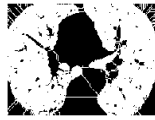
Medical Images	Preprocessed		Ground Truth	Segmented	Cropped Comparison	
	Yes/No	Result			Result	Ground Truth
	Yes					
	No					
	Yes					
	No					

The distinctive improvements in image quality, particularly when comparing images with and without HE preprocessing, underscore the significance of employing appropriate preprocessing methods to enhance the quality of medical image segmentation results. The sharper delineation of object boundaries, as demonstrated in segmented and cropped images, holds substantial value for medical practitioners by contributing to more precise diagnoses and well-informed clinical decisions.

### 4.3.2. Comparison with Other Segmentation Methods

Additionally, we conducted a comparative analysis between the PSO segmentation method and alternative segmentation techniques, such as Otsu, Watershed, and K-means. The findings are presented in Table 5, and they showcase a substantial difference in the segmentation outcomes achieved by our proposed method compared to other techniques. The results suggest that the PSO segmentation approach, when coupled with preprocessing techniques, delivers images with superior clarity and accuracy.

**Table 5.** Comparison of PSO segmentation results with other methods (Otsu, Watershed, and K-Means) on medical images with emphasis on histogram equalization (HE).

No.	Ground Truth	HE	PSO Proposed	Comparison with Other Methods		
				Otsu	Watershed	K-Means
1		Yes				
2		No				
3		Yes				
4		No				

In particular, the Dice similarity coefficient (DSC) and Jaccard index values highly indicate the segmentation method’s performance. The values approaching one indicate a remarkable similarity between the segmented objects and their ground truth, demonstrating the high accuracy and precision of the proposed PSO approach. This reinforces the potential of our method for application in medical image segmentation, where precise delineation of anatomical structures is paramount.

The results suggest that preprocessing techniques, especially HE and the proposed adjustments, contribute significantly to the quality of medical image segmentation. Moreover, when compared to conventional approaches, the PSO segmentation method demonstrates its prowess at producing images with enhanced clarity and accuracy. This is particularly valuable in medical imaging scenarios, where precise segmentation is crucial for diagnosis and treatment planning.

### 4.3.3. Comparison of Our Method with Other Image Preprocessing Approaches Based on Histograms

In our exploration of preprocessing methods, as depicted in Figure 9, traditional histogram equalization (HE) emerges as a straightforward yet robust technique that effectively redistributes pixel intensities to enhance overall contrast. However, its application to medical images reveals inherent drawbacks—notably, the risk of over-amplifying noise and limited adaptability to the diverse characteristics of medical images—thereby constraining its efficacy at preserving critical fine details necessary for medical diagnosis.

Adaptive histogram equalization (AHE) addresses some of HE’s limitations by introducing local contrast adjustments. While successfully handling variable pixel intensities, AHE brings its own challenges, including the potential for artifacts and an in-

creased risk of noise amplification in homogenous regions. These limitations constrain the method's suitability for medical image enhancement and prompt a quest for more sophisticated approaches.

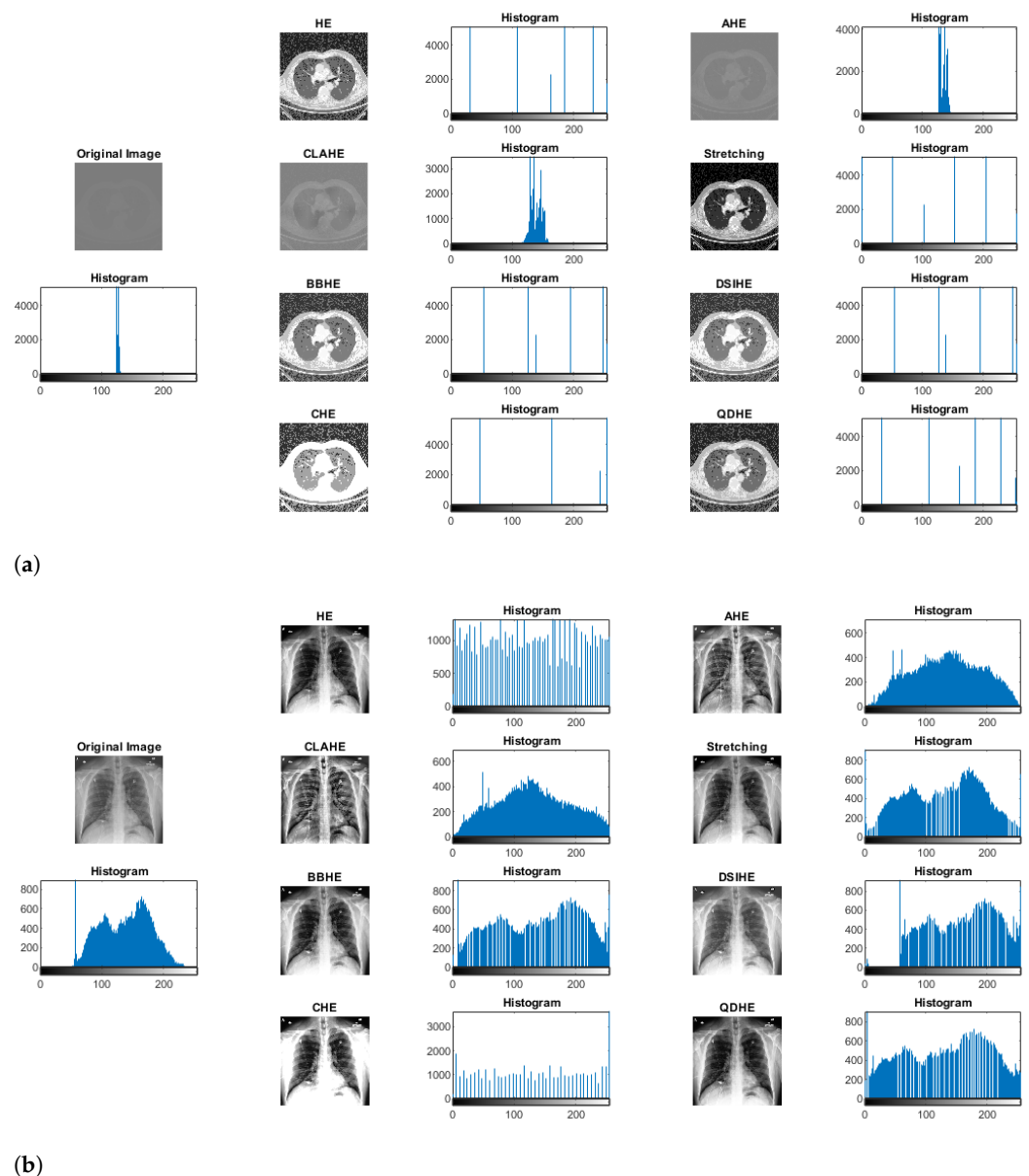


**Figure 9.** Comparison of preprocessing approaches based on histogram analysis with samples of (a) lung CT scans and (b) chest X-rays. The figure illustrates the outcomes of various histogram-based preprocessing methods, including histogram equalization (HE), adaptive histogram equalization (AHE), contrast-limited adaptive histogram equalization (CLAHE), bi-histogram equalization (BBHE), and quadrants dynamic histogram equalization (QDHE).

The evolution continues with contrast-limited adaptive histogram equalization (CLAHE), which improves upon AHE by introducing a clip limit to curb over-amplification. Despite this enhancement, determining an optimal clip limit remains a nuanced task, with artifacts still likely to emerge, especially in large images. Bi-histogram equalization (BBHE) modifies the approach by equalizing two separate histogram parts to mitigate over-amplification issues. However, challenges persist in preserving details within regions exhibiting varying intensity distributions. Cumulative histogram equalization (CHE) is another noteworthy method that dynamically enhances image contrast based on cumu-

lative histograms to provide an alternative approach with advantages and limitations. Finally, the quadrants dynamic histogram equalization (QDHE) method dynamically applies histogram equalization to image quadrants and shows promise for localized adaptation. However, meticulous parameter adjustments are essential to circumvent artifacts, and computational costs may rise.

This comprehensive analysis underpins our innovative integration of histogram equalization with PSO segmentation with the aim of addressing these challenges and optimizing medical image preprocessing.

Table 6 comprehensively evaluates several medical image preprocessing methods applied to lung CT and chest X-ray images. The metrics used for assessment include accuracy, precision, recall, specificity, Dice, and Jaccard. The proposed HE method demonstrates outstanding performance, with a high accuracy of 95.63%. This method effectively enhances lung CT images, providing notable improvements across all evaluated metrics. Traditional HE also stands out, showcasing its simplicity and effectiveness and yielding competitive results for various metrics. CLAHE performs well: balancing contrast enhancement and noise control. AHE shows promise by effectively addressing local contrast variations in lung CT images. The stretching method proves reliable: demonstrating the effectiveness of intensity stretching to enhance contrast and preserve fine details. BBHE and DSIHE methods achieve high accuracy, emphasizing their effectiveness at improving contrast and overall image quality. CHE and QDHE offer alternative enhancement approaches with competitive results and balanced metrics.

**Table 6.** Performance evaluation metrics for different medical image preprocessing methods on lung CT and chest X-ray images.

Medical Image	Pre-Processing	Evaluation Metrics					
		Accuracy	Precision	Recall	Specificity	Dice	Jaccard
Lung CT	Proposed HE	0.9563	0.97529	0.96811	0.93322	0.967	0.9361
	HE	0.94959	0.95632	0.90652	0.92529	0.93075	0.87048
	CLAHE	0.94785	0.95	0.96363	0.91195	0.95922	0.92164
	AHE	0.94905	0.94589	0.96446	0.90638	0.95996	0.92301
	Stretching	0.94959	0.94589	0.95529	0.90652	0.96037	0.92376
	BBHE	0.95553	0.95829	0.96244	0.92594	0.96531	0.93295
	DSIHE	0.95572	0.95858	0.96245	0.92642	0.96547	0.93324
	CHE	0.88164	0.8371	0.91621	0.76431	0.90132	0.82036
	QDHE	0.92889	0.91219	0.93613	0.89228	0.94308	0.85702
Chest X-ray	Proposed HE	0.9065	0.93504	0.93714	0.94691	0.90173	0.89648
	HE	0.90614	0.9342	0.86086	0.94627	0.89603	0.81165
	CLAHE	0.75458	0.69369	0.72702	0.77399	0.70996	0.55034
	AHE	0.82245	0.84244	0.7694	0.87027	0.80426	0.67261
	Stretching	0.88782	0.92061	0.80864	0.92351	0.88225	0.78931
	BBHE	0.88718	0.92101	0.80745	0.92381	0.88171	0.78844
	DSIHE	0.97381	0.93413	0.85782	0.94512	0.89618	0.81189
	CHE	0.88837	0.92938	0.81013	0.92249	0.88263	0.78992
	QDHE	0.90619	0.9321	0.85905	0.94839	0.89638	0.81222

The proposed HE method also performs exceptionally well on chest X-ray images, achieving a high accuracy of 90.65%. Similar to lung CT results, traditional HE demonstrates its effectiveness at enhancing contrast, although it is slightly outperformed by the proposed method. CLAHE faces challenges in chest X-ray images, resulting in slightly lower overall performance, particularly in accuracy. Adaptive histogram equalization (AHE) maintains balanced performance and effectively addresses local contrast variations in chest X-ray images. The stretching method remains competitive, showcasing the usefulness of intensity stretching to enhance chest X-ray images. Bi-histogram equalization (BBHE) achieves comparable results to other methods and provides an alternative for contrast enhancement.

Dynamic histogram equalization (DSIHE) improves contrast and overall image quality for chest X-ray images. Cumulative histogram equalization (CHE) and quadrants dynamic histogram equalization (QDHE) offer alternative enhancement approaches, each with slightly lower overall performance than the other methods.

Based on the comparison, the proposed HE method consistently demonstrates high accuracy and competitive performance for lung CT and chest X-ray images. Additionally, alternative methods such as BBHE, DSIHE, and QDHE are promising, and each has its strengths and applicability area. The choice of preprocessing method may depend on the specific characteristics of the medical images and the desired trade-offs between different evaluation metrics.

#### 4.4. Limitations

While versatile, our proposed integrated PSO and HE method grapples with inherent variability in medical images, including factors like resolution, noise levels, and modality-specific traits. Recognizing these challenges, the method's adaptability across diverse medical imaging scenarios calls for nuanced optimization tailored to specific image intricacies.

Like many optimization-driven techniques, our method's performance relies on well-calibrated parameter settings, especially within the PSO algorithm. Sensitivity to these parameters emphasizes the need for meticulous fine-tuning across datasets and medical imaging contexts. Future research may explore adaptive strategies for parameter adjustment to enhance flexibility and integration across varied medical imaging scenarios.

The integration of PSO with HE introduces computational complexity. While excelling at segmentation accuracy, the associated computational overhead raises considerations for real-time applications and resource-constrained environments. Future optimizations, such as parallelization or algorithmic refinements, are imperative to balance accuracy and computational efficiency.

#### Collaborative Adaptability for Overlapping Structures

Our method encounters unique challenges in chest X-ray images, where overlapping structures challenge traditional image processing methods. Particle swarm optimization (PSO) emerges as a strategic tool to address these intricacies, as it dynamically explores the solution space and adapts to the nuanced features of chest X-ray images.

The swarm intelligence inherent to PSO becomes a key ally in overcoming challenges related to overlapping structures. The collaborative and exploratory nature of the particle swarm enables efficient optimization, even in complex and overlapping regions. By harnessing the collective intelligence of particles, the algorithm navigates intricate spatial relationships, ensuring that overlapping structures do not hinder the segmentation process.

PSO's ability to balance exploration and exploitation proves crucial to address the challenges posed by overlapping structures. The algorithm's iterative nature allows it to explore diverse solutions while exploiting promising regions, which prevents entrapment in local minima. This dynamic balance contributes to the robustness of our proposed method, especially in regions where overlapping structures demand adaptive and nuanced segmentation approaches.

## 5. Conclusions

In this study, we investigated the potential of particle swarm optimization (PSO) as a medical image segmentation method and specifically focused on lung CT scan and chest X-ray images. Our results underscore the significant role of preprocessing techniques, particularly histogram equalization (HE), in shaping the quality and precision of segmented images. HE, when applied, led to a notable improvement in accuracy and Dice in lung CT scan images and elevated the overall segmentation quality. The challenges encountered with chest X-ray images, characterized by lower spatial resolution and the presence of overlapping structures, emphasize the importance of choosing the appropriate segmentation method, especially when HE is not employed. Here, certain alternative techniques

demonstrate competitive performance, highlighting the need to consider image-specific characteristics in the selection process.

Comparative assessments against other segmentation methods, including Otsu, Watershed, and K-means, accentuate the ability of the PSO segmentation approach to generate images with superior clarity and accuracy, particularly when preprocessing is integrated. Dice similarity coefficient (DSC) and Jaccard index values approaching one indicate the high accuracy and precision of the proposed PSO method and signify its potential in medical image segmentation tasks. In future work, the domain of medical image segmentation can benefit from further exploration and integration of machine learning and deep learning approaches. These methodologies, equipped with robust algorithms and vast datasets, have the potential to further enhance the accuracy and efficiency of medical image segmentation, which will provide invaluable support to medical practitioners and researchers for image analysis and diagnosis.

**Author Contributions:** Conceptualization, S.S. and R.D.; Data curation, S.S.; Formal analysis, S.S. and R.D.; Funding acquisition, R.D.; Investigation, S.S.; Methodology, S.S.; Project administration, R.D.; Resources, S.S.; Software, S.S.; Supervision, R.D.; Validation, S.S. and R.D.; Visualization, S.S.; Writing—original draft, S.S. and R.D.; Writing—review and editing, S.S. and R.D. All authors have read and agreed to the published version of the manuscript.

**Funding:** The research presented in this paper was partially supported by funds from the Polish Ministry of Education and Science assigned to AGH University of Krakow. Additionally, it was also partially supported by PLGrid Infrastructure with grant number PLG/2023/016757.

**Institutional Review Board Statement:** Not applicable.

**Informed Consent Statement:** Not applicable.

**Data Availability Statement:** The datasets used in this study are freely available and can be accessed from <https://www.kaggle.com/datasets/kmader/finding-lungs-in-ct-data> and <https://www.kaggle.com/datasets/tawsifurrahman/covid19-radiography-database> (accessed on 23 June 2023).

**Conflicts of Interest:** The authors declare no conflicts of interest.

## References

1. Karagiannis, S.; Magkos, E.; Ntantogian, C.; Cabecinha, R.; Fotis, T. Cybersecurity and Medical Imaging: A Simulation-Based Approach to DICOM Communication. *Appl. Sci.* **2023**, *13*, 10072. [[CrossRef](#)]
2. Waili, A.R.A. Using Convolutional Neural Networks for Edge Detection in Medical Images to Determine Surgery Instrument Tools. *J. Artif. Intell. Mach. Learn. Neural Netw.* **2023**, *3*, 13–25. [[CrossRef](#)]
3. Hao, X.; Yin, L.; Li, X.; Zhang, L.; Yang, R. A Multi-Objective Semantic Segmentation Algorithm Based on Improved U-Net Networks. *Remote Sens.* **2023**, *15*, 1838. [[CrossRef](#)]
4. Ansari, M.Y.; Abdalla, A.; Ansari, M.Y.; Ansari, M.I.; Malluhi, B.; Mohanty, S.; Mishra, S.; Singh, S.S.; Abinshed, J.; Al-Ansari, A.; et al. Practical utility of liver segmentation methods in clinical surgeries and interventions. *BMC Med. Imaging* **2022**, *22*, 97. [[CrossRef](#)]
5. Urban, R.; Haluzová, S.; Strunga, M.; Surovková, J.; Lifková, M.; Tomášik, J.; Thurzo, A. AI-Assisted CBCT Data Management in Modern Dental Practice: Benefits, Limitations and Innovations. *Electronics* **2023**, *12*, 1710. [[CrossRef](#)]
6. Asiri, A.F.; Altuwalah, A.S. The role of neural artificial intelligence for diagnosis and treatment planning in endodontics: A qualitative review. *Saudi Dent. J.* **2022**, *34*, 270–281. [[CrossRef](#)]
7. Vobugari, N.; Raja, V.; Sethi, U.; Gandhi, K.; Raja, K.; Surani, S.R. Advancements in Oncology with Artificial Intelligence—A Review Article. *Cancers* **2022**, *14*, 1349. [[CrossRef](#)]
8. KV, R.; Prasad, K.; Peralam Yegneswaran, P. Segmentation and Classification Approaches of Clinically Relevant Curvilinear Structures: A Review. *J. Med. Syst.* **2023**, *47*, 40. [[CrossRef](#)]
9. Iqbal, S.; Khan, T.M.; Naveed, K.; Naqvi, S.S.; Nawaz, S.J. Recent trends and advances in fundus image analysis: A review. *Comput. Biol. Med.* **2022**, *151*, 106277. [[CrossRef](#)]
10. Wu, R.; Liang, C.; Li, Y.; Shi, X.; Zhang, J.; Huang, H. Self-supervised transfer learning framework driven by visual attention for benign–malignant lung nodule classification on chest CT. *Expert Syst. Appl.* **2023**, *215*, 119339. [[CrossRef](#)]
11. Kaur, C.; Garg, U. Artificial intelligence techniques for cancer detection in medical image processing: A review. *Mater. Today Proc.* **2023**, *81*, 806–809. [[CrossRef](#)]
12. Liu, F.; Chen, L.; Lu, L.; Ahmad, A.; Jeon, G.; Yang, X. Medical image fusion method by using Laplacian pyramid and convolutional sparse representation. *Concurr. Comput. Pract. Exp.* **2020**, *32*, e5632. [[CrossRef](#)]

13. Junn, J.C.; Soderlund, K.A.; Glastonbury, C.M. Imaging of Head and Neck Cancer With CT, MRI, and US. *Semin. Nucl. Med.* **2021**, *51*, 3–12. [[CrossRef](#)] [[PubMed](#)]
14. Dara, O.A.; Lopez-Guede, J.M.; Raheem, H.I.; Rahebi, J.; Zulueta, E.; Fernandez-Gamiz, U. Alzheimer's Disease Diagnosis Using Machine Learning: A Survey. *Appl. Sci.* **2023**, *13*, 8298. [[CrossRef](#)]
15. Chakraborty, S.; Chatterjee, S.; Das, A.; Mali, K. Penalized Fuzzy C-Means Enabled Hybrid Region Growing in Segmenting Medical Images. *Stud. Comput. Intell.* **2020**, *841*, 41–65. [[CrossRef](#)]
16. Ramesh, K.; Kumar, G.; Swapna, K.; Datta, D.; Rajest, S. A Review of Medical Image Segmentation Algorithms. *EAI Endorsed Trans. Pervasive Health Technol.* **2021**, *7*, 169184. [[CrossRef](#)]
17. Yang, C.; Weng, G.; Chen, Y. Active contour model based on local Kullback–Leibler divergence for fast image segmentation. *Eng. Appl. Artif. Intell.* **2023**, *123*, 106472. [[CrossRef](#)]
18. Oulefki, A.; Agaian, S.; Trongtirakul, T.; Kassah Laouar, A. Automatic COVID-19 lung infected region segmentation and measurement using CT-scans images. *Pattern Recognit.* **2021**, *114*, 107747. [[CrossRef](#)]
19. Shaikh, F.; Dehmeshki, J.; Bisdas, S.; Roettger-Dupont, D.; Kubassova, O.; Aziz, M.; Awan, O. Artificial Intelligence-Based Clinical Decision Support Systems Using Advanced Medical Imaging and Radiomics. *Curr. Probl. Diagn. Radiol.* **2021**, *50*, 262–267. [[CrossRef](#)]
20. Mall, P.K.; Singh, P.K.; Srivastav, S.; Narayan, V.; Paprzycki, M.; Jaworska, T.; Ganzha, M. A comprehensive review of deep neural networks for medical image processing: Recent developments and future opportunities. *Healthc. Anal.* **2023**, *4*, 100216. [[CrossRef](#)]
21. Faragallah, O.S.; El-Hoseny, H.; El-Shafai, W.; El-Rahman, W.A.; El-Sayed, H.S.; El-Rabaie, E.S.M.; El-Samie, F.E.A.; Geweid, G.G.N. A Comprehensive Survey Analysis for Present Solutions of Medical Image Fusion and Future Directions. *IEEE Access* **2021**, *9*, 11358–11371. [[CrossRef](#)]
22. Shang, H.; Zhao, S.; Du, H.; Zhang, J.; Xing, W.; Shen, H. A new solution model for cardiac medical image segmentation. *J. Thorac. Dis.* **2020**, *12*, 7298–7312. [[CrossRef](#)] [[PubMed](#)]
23. Saifullah, S.; Dreżewski, R. Enhanced Medical Image Segmentation using CNN based on Histogram Equalization. In Proceedings of the 2023 2nd International Conference on Applied Artificial Intelligence and Computing (ICAAIC), Salem, India, 4–6 May 2023; pp. 121–126. [[CrossRef](#)]
24. Alliou, H.; Sadgal, M.; Elfazziki, A. Optimized control for medical image segmentation: Improved multi-agent systems agreements using Particle Swarm Optimization. *J. Ambient Intell. Humaniz. Comput.* **2021**, *12*, 8867–8885. [[CrossRef](#)]
25. El-Khatib, S.; Skobtsov, Y.; Rodzin, S. Improved Particle Swarm Medical Image Segmentation Algorithm for Decision Making. *Stud. Comput. Intell.* **2020**, *869*, 437–442. [[CrossRef](#)]
26. Eisham, Z.K.; Haque, M.M.; Rahman, M.S.; Nishat, M.M.; Faisal, F.; Islam, M.R. Chimp optimization algorithm in multilevel image thresholding and image clustering. *Evol. Syst.* **2023**, *14*, 605–648. [[CrossRef](#)]
27. Vijh, S.; Sharma, S.; Gaurav, P. Brain Tumor Segmentation Using OTSU Embedded Adaptive Particle Swarm Optimization Method and Convolutional Neural Network. *Lect. Notes Data Eng. Commun. Technol.* **2020**, *32*, 171–194. [[CrossRef](#)]
28. Shehanaz, S.; Daniel, E.; Guntur, S.R.; Satrasupalli, S. Optimum weighted multimodal medical image fusion using particle swarm optimization. *Optik* **2021**, *231*, 166413. [[CrossRef](#)]
29. Saifullah, S.; Dreżewski, R. Modified Histogram Equalization for Improved CNN Medical Image Segmentation. *Procedia Comput. Sci.* **2023**, *225*, 3021–3030. [[CrossRef](#)]
30. Lan, K.; Zhou, J.; Jiang, X.; Wang, J.; Huang, S.; Yang, J.; Song, Q.; Tang, R.; Gong, X.; Liu, K.; et al. Group theoretic particle swarm optimization for multi-level threshold lung cancer image segmentation. *Quant. Imaging Med. Surg.* **2023**, *13*, 1312–1322. [[CrossRef](#)]
31. Naidu, S.; Quadros, A.; Natekar, A.; Parvatkar, P.; Chaman Kumar, K.; Aswale, S. Enhancement of X-ray images using various Image Processing Approaches. In Proceedings of the 2021 International Conference on Technological Advancements and Innovations (ICTAI), Tashkent, Uzbekistan, 10–12 November 2021; pp. 115–120. [[CrossRef](#)]
32. Elyan, E.; Vuttipittayamongkol, P.; Johnston, P.; Martin, K.; McPherson, K.; Moreno-García, C.F.; Jayne, C.; Mostafa Kamal Sarker, M. Computer vision and machine learning for medical image analysis: Recent advances, challenges, and way forward. *Artif. Intell. Surg.* **2022**, *2*, 24–25. [[CrossRef](#)]
33. Abualigah, L.; Habash, M.; Hanandeh, E.S.; Hussein, A.M.; Shinwan, M.A.; Zitar, R.A.; Jia, H. Improved Reptile Search Algorithm by Salp Swarm Algorithm for Medical Image Segmentation. *J. Bionic Eng.* **2023**, *20*, 1766–1790. [[CrossRef](#)] [[PubMed](#)]
34. Khaniabadi, S.M.; Ibrahim, H.; Huqqani, I.A.; Khaniabadi, F.M.; Sakim, H.A.M.; Teoh, S.S. Comparative Review on Traditional and Deep Learning Methods for Medical Image Segmentation. In Proceedings of the 2023 IEEE 14th Control and System Graduate Research Colloquium (ICSGRC), Shah Alam, Malaysia, 5 August 2023; pp. 45–50. [[CrossRef](#)]
35. Jardim, S.; António, J.; Mora, C. Image thresholding approaches for medical image segmentation - short literature review. *Procedia Comput. Sci.* **2023**, *219*, 1485–1492. [[CrossRef](#)]
36. Feng, Y.; Liu, Y.; Liu, Z.; Liu, W.; Yao, Q.; Zhang, X. A Novel Interval Iterative Multi-Thresholding Algorithm Based on Hybrid Spatial Filter and Region Growing for Medical Brain MR Images. *Appl. Sci.* **2023**, *13*, 1087. [[CrossRef](#)]
37. Xie, Y.; Zhang, Z.; Chen, S.; Qiu, C. Detect, Grow, Seg: A weakly supervision method for medical image segmentation based on bounding box. *Biomed. Signal Process. Control* **2023**, *86*, 105158. [[CrossRef](#)]
38. Jaglan, P.; Dass, R.; Duhan, M. A Comparative Analysis of Various Image Segmentation Techniques. *Lect. Notes Netw. Syst.* **2019**, *46*, 359–374. [[CrossRef](#)]

39. Sarhan, A.; Rokne, J.; Alhaji, R. Glaucoma detection using image processing techniques: A literature review. *Comput. Med. Imaging Graph.* **2019**, *78*, 101657. [[CrossRef](#)]
40. Bennai, M.T.; Guessoum, Z.; Mazouzi, S.; Cormier, S.; Mezghiche, M. A stochastic multi-agent approach for medical-image segmentation: Application to tumor segmentation in brain MR images. *Artif. Intell. Med.* **2020**, *110*, 101980. [[CrossRef](#)]
41. Biratu, E.S.; Schwenker, F.; Ayano, Y.M.; Debelee, T.G. A Survey of Brain Tumor Segmentation and Classification Algorithms. *J. Imaging* **2021**, *7*, 179. [[CrossRef](#)]
42. Biratu, E.S.; Schwenker, F.; Debelee, T.G.; Kebede, S.R.; Negera, W.G.; Molla, H.T. Enhanced Region Growing for Brain Tumor MR Image Segmentation. *J. Imaging* **2021**, *7*, 22. [[CrossRef](#)]
43. Naveen, H.M.; Naveena, C.; Manjunath Aradhya, V.N. An approach for classification of lung nodules. *Tumor Discov.* **2023**, *2*, 317. [[CrossRef](#)]
44. Azouz, Z.; Honarvar Shakibaei Asli, B.; Khan, M. Evolution of Crack Analysis in Structures Using Image Processing Technique: A Review. *Electronics* **2023**, *12*, 3862. [[CrossRef](#)]
45. Kheradmandi, N.; Mehranfar, V. A critical review and comparative study on image segmentation-based techniques for pavement crack detection. *Constr. Build. Mater.* **2022**, *321*, 126162. [[CrossRef](#)]
46. Aldoury, R.S.; Al-Saidi, N.M.; Ibrahim, R.W.; Kahtan, H. A new X-ray images enhancement method using a class of fractional differential equation. *MethodsX* **2023**, *11*, 102264. [[CrossRef](#)] [[PubMed](#)]
47. Pradeep Kumar, B.P.; Rangaiah, P.K.B.; Augustine, R. Enhancing Medical Image Reclamation for Chest Samples using B-Coefficients, DT-CWT and EPS Algorithm. *IEEE Access* **2023**, *11*, 113360–113375. [[CrossRef](#)]
48. Zebari, D.A.; Zeebaree, D.Q.; Abdulazeez, A.M.; Haron, H.; Hamed, H.N.A. Improved Threshold Based and Trainable Fully Automated Segmentation for Breast Cancer Boundary and Pectoral Muscle in Mammogram Images. *IEEE Access* **2020**, *8*, 203097–203116. [[CrossRef](#)]
49. Zhang, W.; Zhuang, P.; Sun, H.H.; Li, G.; Kwong, S.; Li, C. Underwater Image Enhancement via Minimal Color Loss and Locally Adaptive Contrast Enhancement. *IEEE Trans. Image Process.* **2022**, *31*, 3997–4010. [[CrossRef](#)] [[PubMed](#)]
50. Majeed, S.H.; Isa, N.A.M. Adaptive Entropy Index Histogram Equalization for Poor Contrast Images. *IEEE Access* **2021**, *9*, 6402–6437. [[CrossRef](#)]
51. Fan, X.; Sun, Z.; Tian, E.; Yin, Z.; Cao, G. Medical image contrast enhancement based on improved sparrow search algorithm. *Int. J. Imaging Syst. Technol.* **2023**, *33*, 389–402. [[CrossRef](#)]
52. Jawdekar, A.; Dixit, M. A Review of Image Enhancement Techniques in Medical Imaging. In *Machine Intelligence and Smart Systems. Algorithms for Intelligent Systems*; Agrawal, S., Kumar Gupta, K., H. Chan, J., Agrawal, J., Gupta, M., Eds.; Springer: Singapore, 2021; pp. 25–33. [[CrossRef](#)]
53. Islam, S.M.; Mondal, H.S. Image Enhancement Based Medical Image Analysis. In Proceedings of the 2019 10th International Conference on Computing, Communication and Networking Technologies (ICCCNT), Kanpur, India, 6–8 July 2019; pp. 1–5. [[CrossRef](#)]
54. Wang, S.; Cao, G.; Wang, Y.; Liao, S.; Wang, Q.; Shi, J.; Li, C.; Shen, D. Review and Prospect: Artificial Intelligence in Advanced Medical Imaging. *Front. Radiol.* **2021**, *1*, 781868. [[CrossRef](#)]
55. Farshi, T.R.; Drake, J.H.; Özcan, E. A multimodal particle swarm optimization-based approach for image segmentation. *Expert Syst. Appl.* **2020**, *149*, 113233. [[CrossRef](#)]
56. Shi, M.; Chen, C.; Liu, L.; Kuang, F.; Zhao, D.; Chen, X. A grade-based search adaptive random slime mould optimizer for lupus nephritis image segmentation. *Comput. Biol. Med.* **2023**, *160*, 106950. [[CrossRef](#)] [[PubMed](#)]
57. Khosla, T.; Verma, O.P. Optimal threshold selection for segmentation of Chest X-Ray images using opposition-based swarm-inspired algorithm for diagnosis of pneumonia. *Multimed. Tools Appl.* **2023**. [[CrossRef](#)]
58. Lakshman Narayana, V.; Lakshmi Patibandla, R.S.M.; Pavani, V.; Radhika, P. Optimized Nature-Inspired Computing Algorithms for Lung Disorder Detection. *Stud. Comput. Intell.* **2023**, *1066*, 103–118. [[CrossRef](#)]
59. de Albuquerque, V.H.C.; Gupta, D.; De Falco, I.; Sannino, G.; Bouguila, N. Special issue on Bio-inspired optimization techniques for Biomedical Data Analysis: Methods and applications. *Appl. Soft Comput.* **2020**, *95*, 106672. [[CrossRef](#)]
60. Shehab, M.; Abualigah, L.; Al Hamad, H.; Alabool, H.; Alshinwan, M.; Khasawneh, A.M. Moth-flame optimization algorithm: Variants and applications. *Neural Comput. Appl.* **2020**, *32*, 9859–9884. [[CrossRef](#)]
61. Yu, Y.; Wang, C.; Fu, Q.; Kou, R.; Huang, F.; Yang, B.; Yang, T.; Gao, M. Techniques and Challenges of Image Segmentation: A Review. *Electronics* **2023**, *12*, 1199. [[CrossRef](#)]
62. Zhang, L.; Lim, C.P. Intelligent optic disc segmentation using improved particle swarm optimization and evolving ensemble models. *Appl. Soft Comput.* **2020**, *92*, 106328. [[CrossRef](#)]
63. Mandave, D.D.; Patil, L.V. Bio-inspired computing algorithms in dementia diagnosis—A application-oriented review. *Results Control Optim.* **2023**, *12*, 100276. [[CrossRef](#)]
64. Nayak, J.; Swapnarekha, H.; Naik, B.; Dhiman, G.; Vimal, S. 25 Years of Particle Swarm Optimization: Flourishing Voyage of Two Decades. *Arch. Comput. Methods Eng.* **2023**, *30*, 1663–1725. [[CrossRef](#)]
65. Dhal, K.G.; Ray, S.; Das, A.; Das, S. A Survey on Nature-Inspired Optimization Algorithms and Their Application in Image Enhancement Domain. *Arch. Comput. Methods Eng.* **2019**, *26*, 1607–1638. [[CrossRef](#)]
66. Kavitha, A.; Chellamuthu, C. Brain tumour detection using self-adaptive learning PSO-based feature selection algorithm in MRI images. *Int. J. Bus. Intell. Data Min.* **2019**, *15*, 71. [[CrossRef](#)]

67. Sarvamangala, D.R.; Kulkarni, R.V. A Comparative Study of Bio-inspired Algorithms for Medical Image Registration. *Stud. Comput. Intell.* **2019**, *687*, 27–44. [CrossRef]
68. Kate, V.; Shukla, P. Image Segmentation of Breast Cancer Histopathology Images Using PSO-Based Clustering Technique. *Lect. Notes Netw. Syst.* **2020**, *100*, 207–216. [CrossRef]
69. Zhao, Y.; Yu, X.; Wu, H.; Zhou, Y.; Sun, X.; Yu, S.; Yu, S.; Liu, H. A Fast 2-D Otsu lung tissue image segmentation algorithm based on improved PSO. *Microprocess. Microsyst.* **2021**, *80*, 103527. [CrossRef]
70. Chakraborty, R.; Sushil, R.; Garg, M.L. An Improved PSO-Based Multilevel Image Segmentation Technique Using Minimum Cross-Entropy Thresholding. *Arab. J. Sci. Eng.* **2019**, *44*, 3005–3020. [CrossRef]
71. Öztürk, c.; Ahmad, R.; Akhtar, N. Variants of Artificial Bee Colony algorithm and its applications in medical image processing. *Appl. Soft Comput.* **2020**, *97*, 106799. [CrossRef]
72. Guo, J.; Ma, J.; García-Fernández, Á.F.; Zhang, Y.; Liang, H. A survey on image enhancement for Low-light images. *Heliyon* **2023**, *9*, e14558. [CrossRef]
73. Liu, L.; Zhao, D.; Yu, F.; Heidari, A.A.; Ru, J.; Chen, H.; Mafarja, M.; Turabieh, H.; Pan, Z. Performance optimization of differential evolution with slime mould algorithm for multilevel breast cancer image segmentation. *Comput. Biol. Med.* **2021**, *138*, 104910. [CrossRef]
74. Alnazer, I.; Bourdon, P.; Urruty, T.; Falou, O.; Khalil, M.; Shahin, A.; Fernandez-Maloigne, C. Recent advances in medical image processing for the evaluation of chronic kidney disease. *Med. Image Anal.* **2021**, *69*, 101960. [CrossRef]
75. Saini, M.; Susan, S. Tackling class imbalance in computer vision: A contemporary review. *Artif. Intell. Rev.* **2023**, *56*, 1279–1335. [CrossRef]
76. Huang, Q.; Ding, H.; Razmjoooy, N. Oral cancer detection using convolutional neural network optimized by combined seagull optimization algorithm. *Biomed. Signal Process. Control* **2024**, *87*, 105546. [CrossRef]
77. Karsa, A.; Punwani, S.; Shmueli, K. An optimized and highly repeatable MRI acquisition and processing pipeline for quantitative susceptibility mapping in the head-and-neck region. *Magn. Reson. Med.* **2020**, *84*, 3206–3222. [CrossRef]
78. Hadjiiski, L.; Cha, K.; Chan, H.; Drukker, K.; Morra, L.; Näppi, J.J.; Sahiner, B.; Yoshida, H.; Chen, Q.; Deserno, T.M.; et al. AAPM task group report 273: Recommendations on best practices for AI and machine learning for computer-aided diagnosis in medical imaging. *Med. Phys.* **2023**, *50*, e1–e24. [CrossRef] [PubMed]
79. Maier-Hein, L.; Eisenmann, M.; Sarikaya, D.; März, K.; Collins, T.; Malpani, A.; Fallert, J.; Feussner, H.; Giannarou, S.; Mascagni, P.; et al. Surgical data science—From concepts toward clinical translation. *Med. Image Anal.* **2022**, *76*, 102306. [CrossRef] [PubMed]
80. Rehman, M.U.; Akhtar, S.; Zakwan, M.; Mahmood, M.H. Novel architecture with selected feature vector for effective classification of mitotic and non-mitotic cells in breast cancer histology images. *Biomed. Signal Process. Control* **2022**, *71*, 103212. [CrossRef]
81. Scott Mader, K. Finding and Measuring Lungs in CT Data. 2017. Available online: <https://www.kaggle.com/datasets/kmader/finding-lungs-in-ct-data> (accessed on 23 June 2023).
82. Rahman, T.; Chowdhury, M.; Khandakar, A. COVID-19 Radiography Database. 2022. Available online: <https://www.kaggle.com/datasets/tawsifurrahman/covid19-radiography-database> (accessed on 23 June 2023).
83. Saifullah, S.; Yuwono, B.; Rustamaji, H.C.; Saputra, B.; Dwiyanto, F.A.; Dreżewski, R. Detection of Chest X-ray Abnormalities Using CNN Based on Hyperparameter Optimization. *Eng. Proc.* **2023**, *56*, 223. [CrossRef]
84. Song, Y.; Ren, S.; Lu, Y.; Fu, X.; Wong, K.K. Deep learning-based automatic segmentation of images in cardiac radiography: A promising challenge. *Comput. Methods Programs Biomed.* **2022**, *220*, 106821. [CrossRef] [PubMed]
85. Saifullah, S.; Dreżewski, R.; Khaliduzzaman, A.; Tolentino, L.K.; Ilyos, R. K-Means Segmentation Based-on Lab Color Space for Embryo Detection in Incubated Egg. *J. Ilm. Tek. Elektro Komput. Dan Inform.* **2022**, *8*, 175–185. [CrossRef]
86. Rehman, M.U.; Ryu, J.; Nizami, I.F.; Chong, K.T. RAAGR2-Net: A brain tumor segmentation network using parallel processing of multiple spatial frames. *Comput. Biol. Med.* **2023**, *152*, 106426. [CrossRef]
87. Masoudi, S.; Harmon, S.A.; Mehralivand, S.; Walker, S.M.; Raviprakash, H.; Bagci, U.; Choyke, P.L.; Turkbey, B. Quick guide on radiology image pre-processing for deep learning applications in prostate cancer research. *J. Med. Imaging* **2021**, *8*, 010901. [CrossRef]
88. Aumann, S.; Donner, S.; Fischer, J.; Müller, F. Optical Coherence Tomography (OCT): Principle and Technical Realization. In *High Resolution Imaging in Microscopy and Ophthalmology*; Springer: Cham, Switzerland, 2019; pp. 59–85. [CrossRef]
89. El-Shafai, W.; Almomani, I.; Ara, A.; Alkhayer, A. An optical-based encryption and authentication algorithm for color and grayscale medical images. *Multimed. Tools Appl.* **2023**, *82*, 23735–23770. [CrossRef]
90. Hoque, M.Z.; Keskinarkaus, A.; Nyberg, P.; Seppänen, T. Stain normalization methods for histopathology image analysis: A comprehensive review and experimental comparison. *Inf. Fusion* **2024**, *102*, 101997. [CrossRef]
91. Nazir, N.; Sarwar, A.; Saini, B.S.; Shams, R. A Robust Deep Learning Approach for Accurate Segmentation of Cytoplasm and Nucleus in Noisy Pap Smear Images. *Computation* **2023**, *11*, 195. [CrossRef]
92. Saifullah, S.; Dreżewski, R.; Yudhana, A.; Pranolo, A.; Kaswijanti, W.; Suryotomo, A.P.; Putra, S.A.; Khaliduzzaman, A.; Prabuwo, A.S.; Japkowicz, N. Nondestructive chicken egg fertility detection using CNN-transfer learning algorithms. *J. Ilm. Tek. Elektro Komput. Dan Inform. (JITEKI)* **2023**, *9*, 854–871.
93. Saifullah, S.; Dreżewski, R. Non-Destructive Egg Fertility Detection in Incubation Using SVM Classifier Based on GLCM Parameters. *Procedia Comput. Sci.* **2022**, *207*, 3254–3263. [CrossRef]

94. Okwu, M.O.; Tartibu, L.K. Particle Swarm Optimisation. In *Metaheuristic Optimization: Nature-Inspired Algorithms Swarm and Computational Intelligence, Theory and Applications*; Springer: Cham, Switzerland, 2021; Volume 927, pp. 5–13. [[CrossRef](#)]
95. Gad, A.G. Particle Swarm Optimization Algorithm and Its Applications: A Systematic Review. *Arch. Comput. Methods Eng.* **2022**, *29*, 2531–2561. [[CrossRef](#)]
96. Djemame, S.; Batouche, M.; Oulhadj, H.; Siarry, P. Solving reverse emergence with quantum PSO application to image processing. *Soft Comput.* **2019**, *23*, 6921–6935. [[CrossRef](#)]
97. Narayan, V.; Faiz, M.; Mall, P.K.; Srivastava, S. A Comprehensive Review of Various Approach for Medical Image Segmentation and Disease Prediction. *Wirel. Pers. Commun.* **2023**, *132*, 1819–1848. [[CrossRef](#)]
98. He, M.; Liu, M.; Wang, R.; Jiang, X.; Liu, B.; Zhou, H. Particle swarm optimization with damping factor and cooperative mechanism. *Appl. Soft Comput.* **2019**, *76*, 45–52. [[CrossRef](#)]
99. Papazoglou, G.; Biskas, P. Review and Comparison of Genetic Algorithm and Particle Swarm Optimization in the Optimal Power Flow Problem. *Energies* **2023**, *16*, 1152. [[CrossRef](#)]
100. Piotrowski, A.P.; Napiorkowski, J.J.; Piotrowska, A.E. Population size in Particle Swarm Optimization. *Swarm Evol. Comput.* **2020**, *58*, 100718. [[CrossRef](#)]
101. Chen, H.I.; Yang, B.; Wang, S.j.; Wang, G.; Liu, D.y.; Li, H.z.; Liu, W.b. Towards an optimal support vector machine classifier using a parallel particle swarm optimization strategy. *Appl. Math. Comput.* **2014**, *239*, 180–197. [[CrossRef](#)]
102. Han, W.; Yang, P.; Ren, H.; Sun, J. Comparison study of several kinds of inertia weights for PSO. In Proceedings of the 2010 IEEE International Conference on Progress in Informatics and Computing, Shanghai, China, 10–12 December 2010. [[CrossRef](#)]
103. Taha, A.A.; Hanbury, A. Metrics for evaluating 3D medical image segmentation: Analysis, selection, and tool. *BMC Med. Imaging* **2015**, *15*, 29. [[CrossRef](#)] [[PubMed](#)]

**Disclaimer/Publisher’s Note:** The statements, opinions and data contained in all publications are solely those of the individual author(s) and contributor(s) and not of MDPI and/or the editor(s). MDPI and/or the editor(s) disclaim responsibility for any injury to people or property resulting from any ideas, methods, instructions or products referred to in the content.